DOI:
10.1002/chem.201701837

Document Version
Peer reviewed version

Induction of necroptosis in cancer stem cells by a nickel(II)-dithiocarbamate phenanthroline complex

Marie Flamme, Paul B. Cressey, Chunxin Lu, Peter M. Bruno, Arvin Eskandari, Michael T. Hemann, Graeme Hogarth, and Kogularamanan Suntharalingam*

Abstract: The cytotoxic properties of a series of nickel(II)-dithiocarbamate phenanthroline complexes is reported. The complexes, **1**-**6** kill bulk cancer cells and cancer stem cells (CSCs) with micromolar potency. Two of the complexes, **2** and **6** kill breast cancer stem cell (CSC)-enriched HMLER-shEcad cells 2-fold better than breast CSC-depleted HMLER cells. Complex **2** inhibits mammosphere formation to a similar extent as salinomycin (a CSC-specific toxin). Detailed mechanistic studies suggest that **2** induces CSC death by necroptosis, a programmed form of necrosis. Specifically, **2** triggers MLKL phosphorylation, oligomerization and translocation to the cell membrane. Further, **2** induces necrosome-mediated propidium iodide (PI) uptake and mitochondrial membrane depolarisation, and morphological changes consistent with necroptotosis. Strikingly, **2** does not evoke necroptosis by intracellular reactive oxygen species (ROS) production or poly ADP ribose polymerase (PARP-1) activation.

Introduction

Most compounds, including metal complexes, that have been investigated as anticancer agents induce cell death by programmed apoptosis and hence are susceptible to classical multi-drug resistance pathways.[1] Only a handful of metal complexes have been reported to induce cell death via non-apoptotic pathways.[2] Characterized non-apoptotic pathways include autophagy, pyroptosis, ferroptosis, and necrosis.[3] Necrosis was originally thought to occur in a random, unregulated manner, however, recent studies have shown that it can proceed in an ordered fashion in certain cell types.[4] The most widely studied and major form of controlled necrosis is necroptosis.[5] Necroptosis hinges on the formation of an amyloid-like fibrillar complex called necrosome, consisting of receptor-interacting protein kinase 1 (RIP1), receptor-interacting protein kinase 3 (RIP3), and mixed lineage kinase domain-like protein (MLKL).[6] The necrosome complex mediates downstream execution processes such as reactive oxygen species (ROS) burst, plasma membrane permeabilisation, mitochondrial membrane depolarisation, and bioenergetics depletion.[6b,7] As necroptosis utilizes protein components that are distinctly different from those used in apoptosis, cancer cells that display apoptosis resistance maybe be susceptible to necroptosis-inducers.[8]

[*] Dr K. Suntharalingam, M. Flamme, P.B. Cressey, Dr C. Lu, A. Eskandari, Dr G. Hogarth
Department of Chemistry
King's College London
London
SE1 1DB, UK
E-mail: kogularamanan.suntharalingam@kcl.ac.uk

Dr M. T. Hemann, P. M. Bruno
The Koch Institute for Integrative Cancer Research
Massachusetts Institute of Technology,
Cambridge
Massachusetts
02139, United States

Supporting information for this article is given via a link at the end of the document.

Multi-drug resistant pathways such as apoptosis dysfunction are operative in cancer stem cells (CSCs).[9] CSCs are a sub-population of tumor cells linked to cancer relapse and metastasis.[10] Due to their stem cell-like properties, CSCs divide in a slow and controlled manner, and thus evade conventional apoptosis-inducing chemotherapies which typically target fast growing cells.[11] Upon surviving initial treatment, CSCs are able to reform tumor masses and generate motile-proficient cancer cells capable of colonizing secondary tumor sites.[12] Therefore, cancer therapies must have the ability to eliminate entire tumor populations, including CSCs, to provide long-lasting durable responses. Potential CSC therapeutic targets, such as deregulated signaling pathways,[13] overactive organelles,[14] cell surface markers,[15] and vulnerable microenvironments[16] have been identified, however, there is still no clinically approved agent that can selectively remove CSCs. Apoptosis-resistant CSCs that possess the necessary protein machinery required for necroptotsis can be theoretically removed by necroptosis-inducers.

Platinum-based cancer drugs, cisplatin, carboplatin, and oxaliplatin, are widely used alone or in combination with other agents to treat various solid tumors, but they are ineffective against CSCs at their therapeutically administered doses.[17] Thus, alternative metal-based drugs with novel mechanisms of action are needed to overcome CSCs and prevent tumor reoccurrence. We and others have recently shown that copper, cobalt, gold, iron, and osmium complexes are able to potently and selectively kill CSCs (over bulk cancer cells).[17a,18] Small molecules containing nickel have been investigated as potential anticancer agents but detailed studies investigating their cellular mechanism of action are extremely rare and there have been no reports on their anti-CSC properties.[19] Nickel(II) complexes containing semicarbazone and thiosemicarbazone ligands exhibit potent in vitro antiproliferative activity and are thought to induce their cytotoxic effect by damaging genomic DNA or inhibiting topoisomerase II.[20] Nickel(II)-tetraazamacrocyclic complexes also display promising in vitro activity against promyelocytic leukemia (HL-60) and hepatocellular carcinoma (BEL-7404) cell lines.[21] These complexes are thought to induce apoptotic cell death by condensing and clumping chromatin, and perturbing cell cycle progression. Nickel(II) complexes containing *N*-aroyl-*N'*-thiohydrazide ligands inhibited Dalton's lymphoma (DL) growth in vitro and prolonged survival of DL bearing mice, partly by reversing tumor associated immunosuppression.[22] More recent studies have shown that a nickel(II)-pyrithione complex is capable of inhibiting the proliferation of cultured tumor cells, primary cells from acute myeloid leukaemia human patients, and chronic myelogenous leukaemia (K562) and lung carcinoma (A549) xenografts in nude mice.[23] Detailed mechanistic studies suggest that the complex acts by inhibiting the ubiquitin-proteasome system (UPS) by targeting the 19S proteasome-associated deubiquitinases, UCHL5 and USP14. Herein we present the bulk cancer cell and CSC potency of a series of nickel(II)-dithiocarbamate phenanthroline complexes, **1**-**6** and the novel necroptotic mechanism of action (in CSCs) of the diethyldithiocarbamate-bearing complex, **2**.

Results and Discussion

Synthesis, Characterization, and Stability in Solution

The nickel(II)-dithiocarbamate phenanthroline complexes, **1**-**6** investigated in this study are depicted in Figure 1. The nickel(II) complexes were prepared by reacting $NiCl_2 \cdot 6H_2O$ with two equivalence of the appropriate sodium dithiocarbamate in water to form the corresponding *bis*(*N*,*N*-dithiocarbamate)nickel(II) derivatives, **7** and **8** (Figure S1), followed by reaction of **7** or **8** with equimolar amounts of 1,10-phenanthroline, 3,4,7,8-tetramethyl-1,10-phenanthroline, or 4,7-diphenyl-1,10-phenanthroline in acetone. The nickel(II) complexes, **1**-**6** were isolated in reasonable yields (44-89%) as dark green solids, and were fully characterized by UV-Vis and infra-red spectroscopy, and elemental analysis (see ESI). The spectroscopic data was fully consistent with previously reported data on nickel(II)-dithiocarbamate phenanthroline complexes.[24] Attachment of the phenanthroline ligands was clearly illustrated by the hypsochromic shift of the broad d-d transition band from 635-640 nm for **7** and **8** to *ca.* 605 nm for **1**-**6** (Figures S2). IR signals corresponding to C-N and C-S bonds (within the *N*,*N*-dithiocarbamate moiety) displayed lower frequencies for **1**-**6** compared to **7** and **8**, further confirming binding of the phenanthroline ligands (see ESI).

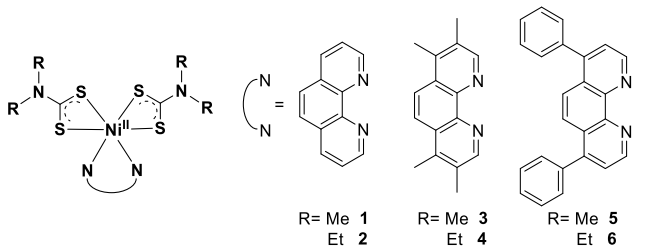

Figure 1. Chemical structures of the nickel(II)-dithiocarbamate phenanthroline complexes, **1**-**6** under investigation.

The lipophilicity of the nickel(II)-complexes, **1**-**6** was determined by measuring the extent to which they partitioned between octanol and water, P. The experimentally determined LogP values for **1**-**6** varied between 0.83-2.71 (Table S1). The hydrophobic nature of the complexes suggests that **1**-**6** will be readily taken up by cells. UV-Vis and high-resolution ESI mass spectroscopy studies were carried out to assess the stability of **2**, taken as a representative member of the nickel(II) series, in solution. NMR stability studies were not preformed given the paramagnetic nature of **2**. The UV-Vis absorption of **2** (50 µM) in DMSO remained consistent over 24 h at 37 °C (Figure S3). Under these conditions, a peak corresponding to the molecular ion of **2** with the appropriate isotopic distribution (534.0561 *m*/*z*) was observed in the positive mode of the ESI mass spectrum (Figure S4). In PBS:DMSO (300:1) containing whole cell lysate (5×10^3 HMLER-shEcad cells) a marked decrease in the MLCT/LMCT absorption bands (> 300 nm) and a concurrent increase in the high energy band at 264 nm was observed (Figure S5), yielding a UV-Vis trace indicative of free 1,10-phenanthroline (Figure S6). Under these conditions, the molecular ion peak for **2** was not observed, however, a new ion peak corresponding to [1,10-phenanthroline-H]$^+$ (179.0197 *m*/*z*) appeared in the positive mode of the ESI mass spectrum (Figure S7). This suggests that 1,10-phenanthroline is displaced from **2**, possibly through interactions with nucleophilic biomolecules present in the cell lysate. Before carrying out cellular studies, the stability of **2** in mammary epithelial cell growth medium (MEGM) was assessed. In MEGM:DMSO (300:1), **2** (50 µM) is stable for up to 18 h at 37 °C (Figure S8). After 18 h, a marked decrease in absorption was observed (Figure S8). Upon incubation of **2** (50 µM) in MEGM for 24 h at 37 °C, a new ion peak corresponding to [1,10-phenanthroline-H]$^+$ (179.0071 *m*/*z*) appeared in the positive mode of the ESI mass spectrum (Figure S9). This suggests that 1,10-phenanthroline is displaced from **2** after prolonged incubation in MEGM.

Cytotoxicity Against Cancer Cells and CSCs

The anti-proliferative properties of **1**-**6** were initially assessed against a panel of human cancer cell lines (MDA-MB-231, HeLa, and U2OS cells) using the MTT [3-(4,5-dimethylthiazol-2-yl)-2,5-diphenyltetrazolium bromide] assay. Cisplatin was included as a positive control. The IC_{50} values (concentrations required to reduce cell viability by 50%) were derived from dose-response curves (Figure S10-13) and are summarized in Table 1 and S2. Complexes **1**-**6** displayed micromolar toxicities, comparable to, and in some cases better than, that of cisplatin. Notably the IC_{50} value of **6** is 11-fold lower against breast adenocarcinoma MDA-MB-231 cells than the IC_{50} value of cisplatin. In general, complexes containing diethyldithiocarbamate (**2**, **4**, and **6**) displayed higher potency than the corresponding complexes with dimethyldithiocarbamate (**1**, **3**, and **5**). The cytotoxicity against breast CSC-enriched cells (HMLER-shEcad) and bulk breast cancer cells (HMLER) was also determined (Figure S14-15 and Table 1). All complexes displayed micromolar toxicity towards HMLER and HMLER-shEcad cells. Strikingly, the diethyldithiocarbamate-bearing complexes, **2** and **6** exhibited 2-fold selective potency for CSCs over bulk cancer cells. This is comparable to salinomycin, a breast CSC-specific compound identified from a high-throughput screen (3-fold),[25] and a series of copper(II)–phenanthroline complexes containing nonsteroidal anti-inflammatory drugs (NSAIDs) recently reported by our group (3-fold).[18a,18c] Although salinomycin displays better potency and selectivity for CSCs than complex **2**, complex **2** exhibits a significantly larger toxicity differential (the concentration difference between the IC_{50} values for HMLER and HMLER-shEcad cells).

Table 1. IC_{50} values of the nickel(II)-dithiocarbamate phenanthroline complexes, **1**-**6**, cisplatin and salinomycin against MDA-MB-231, HMLER cells, and HMLER-shEcad cells.

Compound	MDA-MB-231 IC_{50} [µM] [a]	HMLER IC_{50} [µM] [a]	HMLER-shEcad IC_{50} [µM] [a]
1	41.4 ± 6.2	22.3 ± 6.2	25.2 ± 5.5
2	10.9 ± 0.6	42.8 ± 4.3	21.6 ± 3.2
3	20.1 ± 0.8	11.6 ± 0.7	32.8 ± 5.2
4	7.8 ± 0.7	3.1 ± 0.3	6.0 ± 0.2
5	5.7 ± 0.4	3.6 ± 0.1	5.0 ± 0.1
6	3.3 ± 1.2	4.65 ± 0.2	2.3 ± 0.2
cisplatin	36.6 ± 2.0	3.4 ± 0.5 [b]	4.9 ± 0.4 [b]
salinomycin	n.d.	16.4 ± 2.1 [b]	5.6 ± 0.1 [b]

[a] Determined after 72 h incubation (mean of three independent experiments ± SD). [b] Reported in reference 18c. n.d. not determined.

When breast CSCs are grown under low-attachment conditions in serum-free media, three-dimensional, tumour-like structures called mammospheres can be formed.[26] These structures provide a reliable in vitro model to probe CSC activity. The ability of **2** and **6** (the CSC-selective complexes) to inhibit HMLER-shEcad mammosphere formation from single cell

suspensions at non-lethal doses was determined using an inverted microscope (Figure 2A-B). Dosage with **2** (at the IC_{20} value after 5 days incubation) markedly reduced the number and size of mammospheres formed (Figure 2A-B). A similar result was previously observed for salinomycin.[18a] Treatment with **6** and cisplatin (at the IC_{20} value after 5 days incubation) did not significantly (p = 0.13 for **6** and p = 0.21 for cisplatin) reduce the number of mammospheres formed, however, the size of the mammospheres was noticeably reduced, albeit to a lesser extent than with **2** (Figure 2A-B). This data shows that **2** not only kills breast CSCs preferentially over bulk breast cancer cells, but also reduces mammosphere formation and growth.

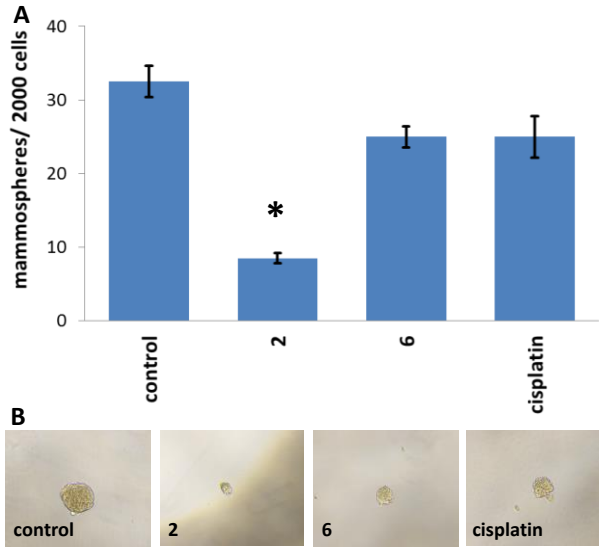

Figure 2. (A) Quantification of mammosphere formation with HMLER-shEcad cells untreated and treated with **2**, **6**, and cisplatin at their respective IC20 values for 5 days. Error bars = SD and Student t-test, * = $p < 0.05$. (B) Representative bright-field images (× 10) of the mammospheres in the absence and presence of **2**, **6**, and cisplatin, at their respective IC_{20} values.

Cellular uptake by CSCs

Cellular uptake studies were performed to elucidate the cell permeability of **1**-**6**. HMLER-shEcad cells were incubated with **1**-**6** (10 µM) for 24 h and the intracellular nickel content was determined by inductively coupled plasma mass spectrometry (ICP-MS). The complexes, **1**-**6** were readily internalized by cells, with whole cell uptake ranging from 575 ppb of Ni/ million cells for **3** to 997 ppb of Ni/ million cells for **6** (Figure S16). A moderate correlation was observed between lipophilicity (LogP) and cell uptake. The 1,10-phenanthroline- and 3,4,7,8-tetramethyl-1,10-phenanthroline-bearing complexes, **1**-**4**, with Log P values ranging from 0.83-1.66, were internalized to a lesser extent than the 4,7-diphenyl-1,10-phenanthroline-containing complexes, **5** and **6**, with Log P values ranging from 2.12-2.71. Nickel(II) complexes containing diethyldithiocarbamate (**2**, **4**, and **6**) were taken up better than the corresponding complexes with dimethyldithiocarbamate (**1**, **3**, and **5**). A similar trend was also observed for HMLER-shEcad cell cytotoxicity (*vide supra*). Time dependent cellular uptake studies, over the course of 72 h, suggest that **2** is almost entirely taken up by HMLER-shEcad cells within 12 h of incubation (Figure S17).

Mechanism of Action Studies

To determine the mechanism of action of **2**, the most effective anti-CSC complex based on monolayer and mammosphere studies, we utilized a mechanism of action predictive functional genetic assay based on RNAi.[27] This methodology relies on the response of eight murine lymphoma cell lines each harboring a distinct shRNA. Treatment of these cell lines with a compound of interest at equipotent concentrations, elicits a pattern of responses (or signature) that is unique to the mechanism of action of that given compound. Thus, when examining a new compound, one can compare its signature to those in the reference set, which includes nearly all classes of clinically used cytotoxins as well as more recently developed targeted therapeutics. When the RNAi signature of a given compound does not match any of the mechanism of action categories in the reference set, the relative similarities to compounds in the reference set, or those in the database but not in the reference set, can be used to gain insight into the mechanism of action. Using this approach, we found that the RNAi signature of **2** did not resemble any of the signatures in the reference set, and thus its mechanism of action was classified as a "new class" (Figure 3A). Next, we calculated the average of the absolute sum of the Euclidian distances between the RNAi signature of **2** and compounds not part of the reference set but in our database. This analysis revealed similar signatures between **2** and shikonin (Euclidian distance = 0.88, p-value = 0.11), a well-established necroptosis inducer, and two rhenium(V)-oxo complexes (Euclidian distance = 1.51 and 1.91) previously characterized as ROS-inducing, necroptotic agents (Figure 3A).[2d,28] Comparison of the Euclidian distances between the RNAi signature of **2** and those of previously reported metal-based CSC-selective agents[17a,18a-c] (**Os-1**, **Cu-1-4**, and **Co-1**, see Figure S18-19) revealed that their mechanisms of action were largely unrelated (Figure 3B). This was somewhat expected as **Os-1**, **Cu-1**-**4**, and **Co-1** induce CSC death by apoptosis. A moderate correlation between the mechanism of action of **2** and **Cu-1** was observed (Euclidian distance = 2.240). Overall the RNAi signature analysis suggests that **2** induces necroptosis and that its mechanism of action is distinct from other metal-based CSC-selective agents.

To verify the mode of cell death evoked by **2**, cytotoxicity studies were performed with HMLER-shEcad cells in the presence of necrosis and apoptosis inhibitors. Co-incubation of **2** with IM-54 (10 µM), an inhibitor of unregulated necrosis mediated by oxidative stress,[29] did not significantly affect the toxicity of **2** (p = 0.19) (Figure 3C), indicating that **2** does not induce unregulated necrosis. Distinct from unregulated necrosis, necroptosis, is a highly ordered form of necrosis that relies on the formation of necrosomes which initiate cell death. Necroptosis is inhibited by necrostatin-1 and dabrafenib, small molecule inhibitors of RIP1 and RIP3 respectively.[30] Co-incubation of **2** with necrostatin-1 (20 µM) or dabrafenib (10 µM), significantly ($p < 0.01$) decreased the toxicity of **2** against HMLER-shEcad cells (Figure 3C). A similar effect was also observed for shikonin in the presence of necrostatin-1 or dabrafenib (Figure S20). This suggests that **2** may induce necrosome-mediated necroptotic cell death. Immunoblotting studies showed that the necrosome components; RIP1, RIP3, and MLKL are expressed in HMLER-shEcad cells, and that their expression levels remain largely unaltered upon treatment with **2** (10 - 20 µM for 72 h; Figure S21). This suggests that **2**-induced necroptosis in HMLER-shEcad cells relies on RIP1-RIP3-MLKL association, and not on the expression levels of the individual protein kinases. Co-incubation of **2** with z-VAD-FMK (5 µM), a potent inhibitor of caspase-dependent apoptosis,[31] slightly increased **2** potency towards HMLER-shEcad cells (Figure 3C). This suggests that blocking apoptosis in CSCs enhances **2**-induced cell death. Similar enhancements in potency in the presence of z-VAD-FMK have been reported for other necroptosis-inducing agents.[2d,32] As expected, the CSC potency of cisplatin, an established apoptosis-inducing agent, significantly decreased ($p < 0.05$) in the presence of z-VAD-FMK (Figure S22). Immunoblotting studies showed that the expression of proteins associated with apoptotic cell death, namely, cleaved caspases 3 and 7 did not increase in HMLER-shEcad cells treated

with **2** (10 - 20 µM for 72 h; Figure S21), providing further evidence for non-apoptotic cell death. Collectively, the cytotoxicity and immunoblotting data for **2** is consistent with the mechanism of action derived from the RNAi-based assay.

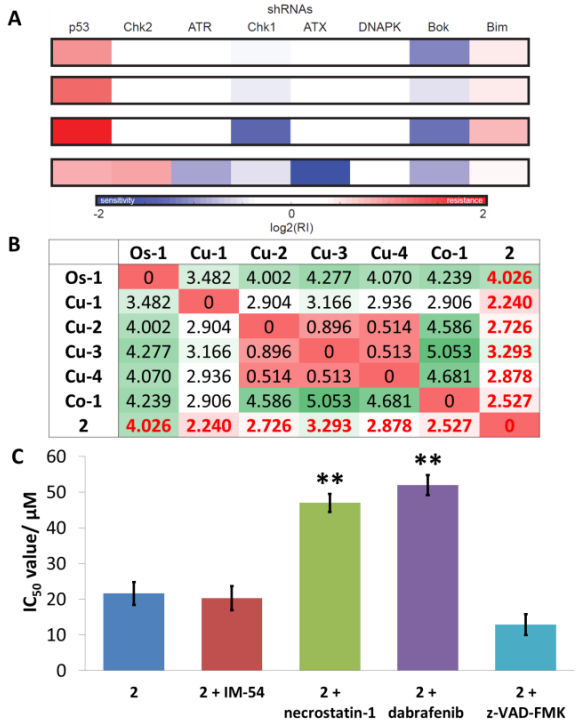

	Os-1	Cu-1	Cu-2	Cu-3	Cu-4	Co-1	2
Os-1	0	3.482	4.002	4.277	4.070	4.239	4.026
Cu-1	3.482	0	2.904	3.166	2.936	2.906	2.240
Cu-2	4.002	2.904	0	0.896	0.514	4.586	2.726
Cu-3	4.277	3.166	0.896	0	0.513	5.053	3.293
Cu-4	4.070	2.936	0.514	0.513	0	4.681	2.878
Co-1	4.239	2.906	4.586	5.053	4.681	0	2.527
2	4.026	2.240	2.726	3.293	2.878	2.527	0

Figure 3. (A) RNAi signatures derived from the treatment of Eµ-Mycp19arf−/− lymphoma cells with **2**, shikonin, [ReO(OMe)(3,4,7,8-tetramethyl-1,10-phenanthroline)Cl_2], and [ReO(OMe)(4,7-diphenyl-1,10-phenanthroline)Cl_2] (top to bottom) at the LD80−90 concentration for each compound. (B) Euclidian distances between the RNAi signatures of **2** and previously reported metal-based CSC-selective agents. Red indicates correlation and green indicates no correlation. (C) Graphical representation of the IC_{50} values of **2** against HMLER-shEcad cells in the absence and presence of IM-54 (10 µM), necrostatin-1 (20 µM), dabrafenib (10 µM), or z-VAD-FMK (5 µM). Error bars represent standard deviations and Student *t-test*, * = $p < 0.01$.

Necroptosis Features in CSCs

Recent studies have shown that necrosome formation triggers MLKL phosphorylation and homo-oligomerization.[6a,33] MLKL homo-oligomers can migrate from the cytoplasm to the cell membrane and induce ion flux, leading to plasma membrane permeabilization.[6a,33] MLKL phosphorylation and oligomerization was observed in HLMER-shEcad cells treated with **2** (10-20 µM for 72 h) (Figure S21). Immunoblotting analysis of the membrane and cytosol fractions of HMLER-shEcad cells treated with **2** (20-40 µM for 24 h) indicated translocation of MLKL to the plasma membrane (Figure S23). To determine if **2** induces necrosome-mediated, MLKL-induced plasma membrane permeabilization, propidium iodide (PI) staining studies were undertaken using flow cytometry. In the absence of permeabilization agents, PI accumulates in, and stains necrotic cells due to their compromised cell membranes. Cells undergoing early-stage apoptosis maintain their cell membrane integrity and thus are not stained by PI. HMLER-shEcad cells treated with **2** (40 µM for 24 h) displayed increased PI uptake relative to untreated cells, suggestive of necrotic cell death (Figure 4A). A similar result was also observed for shikonin (100 nM for 24 h) dosed cells (Figure S23). In the presence of necrostatin-1 (20 µM), dabrafenib (10 µM), or necrosulfonamide (2.5 µM, a small molecule inhibitor of MLKL oligomerization and migration)[34], **2**- and shikonin-mediated PI uptake was partially blocked (Figure 4A and S24). This suggests that **2**-induced plasma membrane permeabilization is associated to necrosome formation and MLKL oligomerization/migration. Other morphological changes associated to necroptosis include cell volume expansion, increase in size of certain organelles, and preservation of the nuclear membrane. Microscopy studies with **2**-treated (20 µM for 24 h) HMLER-shEcad cells revealed a clear loss of plasma membrane integrity and intact nuclear membrane (Figure 4B and S25), consistent with necroptotic cell death.

Necrosomes can induce cell death through mitochondrial membrane depolarization.[35] To determine the effect of **2** on the mitochondrial membrane potential, the JC-1 assay (5,5′,6,6′-tetrachloro-1,1′,3,3′-tetraethylbenzimidazolylcarbocyanine iodide) was employed. JC-1 is a membrane-permeable, cationic, lipophilic dye which accumulates in the mitochondria of healthy cells, forming red light emitting (*ca.* 590 nm) J-aggregates.[76] If the mitochondrial membrane is disrupted, JC-1 forms green light emitting (*ca.* 529 nm) monomers.[36] Therefore, mitochondrial depolarisation is indicated by a reduction in the red-green fluorescence intensity ratio. Upon incubation of HMLER-shEcad cells with **2** (20 µM for 24 h) a marked increase in the population of cells displaying mitochondrial membrane depolarisation was observed (Figure 4C and 4E). A similar trend was detected for HMLER-shEcad cells treated with carbonyl cyanide *m*-chlorophenyl hydrazone (CCCP) (1 µM for 24 h), an established mitochondrial membrane depolarizer (Figure 4D). When **2** was co-incubated with necrostatin-1 (20 µM), mitochondrial membrane depolarisation was attenuated (Figure 4F), suggesting that **2**-induced mitochondrial dysfunction is related to necrosome formation.

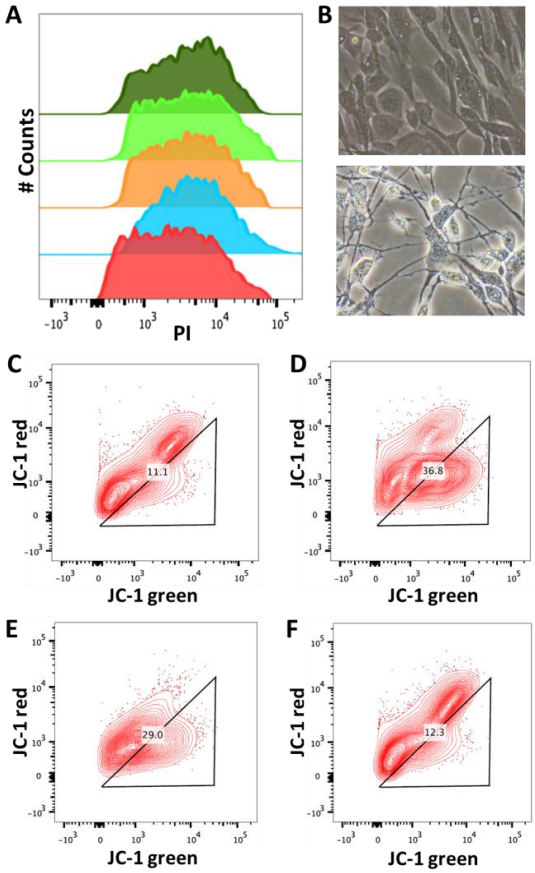

Figure 4. (A) Representative histograms displaying the fluorescence emitted by PI stained HMLER-shEcad cells (red), and HMLER-shEcad cells treated with **2** (40 µM for 24 h) (blue), **2** (40 µM for 24 h) with nectrostatin-1 (20 µM for 24 h) (orange), **2** (40 µM for 24 h) with dabrafenib (10 µM for 24 h) (light green), or **2** (40 µM for 24 h) with necrosulfonamide (2.5 µM for 24 h) (dark green). (B)

Representative bright-field image (× 40) of untreated HMLER-shEcad cells (top) and HMLER-shEcad cells treated with **2** (20 μM for 24 h) (bottom). (C) Representative 2D plots displaying the fluorescence emitted by JC-1 aggregates (red) and JC-1 monomers (green) by untreated HMLER-shEcad cells, (D) HMLER-shEcad cells treated with CCCP (1 μM for 24 h), (E) HMLER-shEcad cells treated with **2** (20 μM for 24 h), (F) HMLER-shEcad cells treated with **2** (20 μM for 24 h) and nectrostatin-1 (20 μM for 24 h).

ROS- and PARP-Independent CSC Death

Another feature of necrosome-mediated cell death is the generation of intracellular reactive oxygen species (ROS).[37] To determine if **2**-induced cell death occurs via ROS production, intracellular ROS levels were quantified using 6-carboxy-2',7'-dichlorodihydrofluorescein diacetate (DCFH-DA), a well-established ROS indicator. HMLER-shEcad cells treated with **2** (40 μM for 6, 12, and 24 h) did not show a noticeable change in intracellular ROS levels compared to untreated cells (Figure S26). In contrast, H_2O_2 (150 μM for 6, 12, and 24 h) treated HMLER-shEcad cells exhibited a significant increase ($p < 0.05$) in ROS levels, which was attenuated in the presence of *N*-acetylcysteine (2.5 mM, a ROS scavenger) (Figure S26). Taken together, this suggests that **2**-induced cell death is not due to ROS generation and moreover, the mechanism of action of **2** does not involve necrosome-mediated ROS.

Hyperactivation of PARP-1, a chromatin-associated enzyme involved in DNA repair, can also trigger necroptosis.[38] DNA damage can activate PARP-1, leading to ATP and NAD depletion and bioenergetics mediated cell death. Necrosome formation is thought to be a potential intermediate step that follows PARP-1 activation.[39] To determine if PARP-1 activation plays a role in **2**-induced cell death, cytotoxicity studies were conducted in the presence of PARP-1 inhibitors, veliparib (ABT-888, 10 μM)[40] and 4-amino-1,8-naphthalimide (ANA, 10 μM).[41] A statistically significant decrease in the potency of **2** towards HMLER-shEcad cells in the presence of the PARP-1 inhibitors was not observed ($p = 0.49$ for ABT-888 and ANA increased potency) (Figure S27), implying that **2**-induced cell death is independent of PARP-1 activity. As expected, the cytotoxicity of cisplatin, a PARP-1 activator,[42] was significantly ($p < 0.05$) reduced in the presence of ABT-888 and ANA (Figure S28). The cytotoxicity data is consistent with immunoblotting studies, which show that **2**-treatment (10 - 20 μM for 72 h) did not upregulate phosphorylated H2AX (γH2AX), a canonical marker for DNA damage (Figure S21).

Conclusions

In summary, we report a series of nickel(II)-dithiocarbamate phenanthroline complexes, **1**-**6** with anticancer potential. Complex **2** and **6** display CSC-selective toxicity, and complex **2** inhibits CSC mammosphere formation to a similar extent as salinomycin, and better than **6** and cisplatin. Mechanistic studies show that **2** induces necroptosis in breast CSCs by necrosome-mediated cell membrane disruption and mitochondrial membrane depolarization. Morphological changes consistent with necroptosis were also observed in **2**-treated CSCs. Interestingly, **2** does not induce necroptosis by elevating intracellular ROS levels or PARP-1 activity. As apoptosis-inducing anticancer agents are widely used to treat cancer patients, the incidence of apoptosis resistance in tumors is becoming more prevalent. Apoptosis resistance is also a hallmark of CSCs. Therefore, compounds such as **2**, which can evoke cell death via novel non-apoptotic pathways could hold the key to overcoming apoptosis resistant CSCs. Given that several metal complexes exhibit toxicity in the micromolar range, the anticancer credibility of these complexes including those presented here need to be validated in animal models. We aim to initiate in vivo studies with the nickel(II) complexes in the future. Overall, our findings could pave the way for the development of other non-apoptosis-inducing metal complexes for CSC-directed chemotherapy.

Experimental Section

Materials and Methods. All synthetic procedures were performed under normal atmospheric conditions. Fourier transform infrared (FTIR) spectra were recorded with a IRAffinity-1S Shimadzu spectrophotometer. UV-Vis absorption spectra were recorded on a Cary UV-vis spectrophotometer. Elemental analysis of the compounds prepared was performed commercially by London Metropolitan University. 1,10-Phenanthroline, 3,4,7,8-tetramethyl-1,10-phenanthroline and 4,7-diphenyl-1,10-phenanthroline were purchased from Sigma Aldrich and used as received. The *bis*(*N*,*N*-dithiocarbamate)nickel(II) derivatives, **7** and **8** were prepared used reported protocols.[43]

Synthesis of Ni(*N*,*N*-dimethyldithiocarbamate)$_2$(1,10-phenanthroline) (1): *Bis*(*N*,*N*-dimethyldithiocarbamate)nickel(II), **7** (48 mg, 0.16 mmol) was dissolved in acetone (5 mL) and added to 1,10-phenanthroline (29 mg, 0.16 mmol). The solution was stirred at 50 ºC for 3 h. The resulting precipitate was filtered, washed with acetone (10 mL) and water (10 mL), and dried. The isolated product was a dark green solid. (64 mg, 83%); UV (chloroform, nm): 387, 321, 289, 270, 248; IR (solid, cm^{-1}): 2916, 2849, 1716, 1493, 1424, 1373, 1338, 1249, 1222, 1197, 1125, 1049, 1024, 979, 901, 850, 809, 781, 727, 722, 639, 577, 442; Anal. Calcd. for **1**, $C_{18}H_{20}N_4NiS_4$ (%): C, 45.11; H, 4.21; N, 11.69. Found: C, 45.21; H, 3.96; N, 11.53.

Synthesis of Ni(*N*,*N*-diethyldithiocarbamate)$_2$(1,10-phenanthroline) (2): *Bis*(*N*,*N*-diethyldithiocarbamate)nickel(II), **8** (82 mg, 0.23 mmol) was dissolved in acetone (5 mL) and added to 1,10-phenanthroline (41 mg, 0.23 mmol). The solution was stirred at 50 ºC for 3 h. The resulting precipitate was filtered, washed with acetone (10 mL) and water (10 mL), and dried. The isolated product was a dark green solid. (69 mg, 57%); UV (chloroform, nm): 390, 325, 290, 270, 250; IR (solid, cm^{-1}): 2968, 2930, 1622, 1586, 1576, 1508, 1477, 1452, 1416, 1372, 1357, 1340, 1305, 1266, 1210, 1135, 1067, 1050, 911, 866, 851, 811, 777, 729, 721, 638, 565; Anal. Calcd. for **2**, $C_{22}H_{28}N_4NiS_4$ (%): C, 49.35; H, 5.27; N, 10.46. Found: C, 49.18; H, 5.04; N, 10.41.

Synthesis of Ni(*N*,*N*-dimethyldithiocarbamate)$_2$(3,4,7,8-tetramethyl-1,10-phenanthroline) (3): *Bis*(*N*,*N*-dimethyldithiocarbamate)nickel(II), **7** (18 mg, 0.06 mmol) was dissolved in acetone (5 mL) and added to 3,4,7,8-tetramethyl-1,10-phenanthroline (14 mg, 0.06 mmol). The solution was stirred at 50 ºC for 3 h. The resulting precipitate was filtered, washed with acetone (10 mL) and water (10 mL), and dried. The isolated product was a dark green solid. (24 mg, 76%); UV (chloroform, nm): 396, 330, 276, 249; IR (solid, cm^{-1}): 2920, 1499, 1426, 1370, 1256, 1241, 1128, 982, 886, 863, 823, 729, 621, 571, 527, 448; Anal. Calcd. For **3**, $C_{22}H_{28}N_4NiS_4$ (%): C, 49.35; H, 5.27; N, 10.46. Found: C, 49.15; H, 5.26; N, 10.35.

Synthesis of Ni(*N*,*N*-diethyldithiocarbamate)$_2$(3,4,7,8-tetramethyl-1,10-phenanthroline) (4): *Bis*(*N*,*N*-diethyldithiocarbamate)nickel(II), **8** (57 mg, 0.16 mmol) was dissolved in acetone (5 mL) and added to 3,4,7,8-tetramethyl-1,10-phenanthroline (38 mg, 0.16 mmol). The solution was stirred at 50 ºC for 3 h. The resulting precipitate was filtered, washed with acetone (10 mL) and water (10 mL), and dried. The isolated product was a dark green solid. (42 mg, 44%); UV (chloroform, nm): 384, 319, 276, 250; IR (solid, cm^{-1}): 2969, 2927, 1481, 1456, 1420, 1373, 1358, 1306, 1268, 1241, 1212, 1139, 1075, 996, 914, 846, 815, 777, 724, 528; Anal. Calcd. for **4**, $C_{26}H_{36}N_4NiS_4$ (%): C, 52.79; H, 6.13; N, 9.47. Found: C, 52.60; H, 5.95; N, 9.32.

Synthesis of Ni(*N*,*N*-dimethyldithiocarbamate)$_2$(4,7-diphenyl-1,10-phenanthroline) (5): *Bis*(*N*,*N*- dimethyldithiocarbamate)nickel(II), **7** (48 mg, 0.16 mmol) was dissolved in acetone (5 mL) and added to 4,7-diphenyl-1,10-phenanthroline (53 mg, 0.16 mmol). The solution was stirred at 50 ^{o}C for 3 h. The resulting precipitate was filtered, washed with acetone (10 mL) and water (10 mL), and dried. The isolated product was a dark green solid (90 mg, 89%); UV (chloroform, nm): 385, 314, 280, 251; IR (solid, cm^{-1}): 1616, 1492, 1418, 1380, 1252, 1228, 1133, 979, 856, 832, 797, 738, 711, 701, 630, 576, 547, 493, 445; Anal. Calcd. for **5**, $C_{30}H_{28}N_4NiS_4$ (%): C, 57.06; H, 4.47; N, 8.87. Found: C, 56.81; H, 4.28; N, 8.84.

Synthesis of Ni(*N*,*N*-diethyldithiocarbamate)$_2$(4,7-diphenyl-1,10-phenanthroline) (6): *Bis*(*N*,*N*-diethyldithiocarbamate)nickel(II), **8** (60 mg, 0.17 mmol) was dissolved in acetone (5 mL) and added to 4,7-diphenyl-1,10-phenanthroline (57 mg, 0.17 mmol). The solution was stirred at 50 ^{o}C for 3 h. The resulting precipitate was filtered, washed with acetone (10 mL) and water (10 mL), and dried. The isolated product was a dark green solid. (61 mg, 52%); UV (chloroform, nm): 387, 317, 283, 250; IR (solid, cm^{-1}): 1617, 1559, 1476, 1416, 1355, 1263, 1209, 1134, 993, 910, 860, 769, 763, 739, 702, 629, 575, 548; Anal. Calcd for **6**, $C_{34}H_{36}N_4NiS_4$ (%): C, 59.39; H, 5.28; N, 8.15. Found: C, 59.18; H, 5.64; N, 8.24.

Measurement of Water-Octanol Partition Coefficient (Log P). The log P value for **1**-**6** was determined using the shake-flask method and UV-Vis spectroscopy. The octanol used in this experiment was pre-saturated with water. An aqueous solution of **1**-**6** (500 µL, 100 µM) was incubated with octanol (500 µL) in a 1.5 mL tube. The tube was shook at room temperature for 48 h. The two phases were separated by centrifugation and **1**-**6** content in each phase was determined by UV-Vis spectroscopy.

Cell Lines and Cell Culture Conditions. U2OS bone osteosarcoma, MDA-MB-231 breast adenocarcinoma, and HeLa cervical adenocarcinoma cell lines were acquired from the American Type Culture Collection (ATCC, Manassas, VA, USA) and maintained in Dulbecco's Modified Eagle's Medium (DMEM) supplemented with 10% fetal bovine serum and 1% penicillin/streptomycin. The human mammary epithelial cell lines, HMLER and HMLER-shEcad were kindly donated by Prof. R. A. Weinberg (Whitehead Institute, MIT). HMLER and HMLER-shEcad cells were maintained in Mammary Epithelial Cell Growth Medium (MEGM) with supplements and growth factors (BPE, hydrocortisone, hEGF, insulin, and gentamicin/amphotericin-B). The cells were grown at 310 K in a humidified atmosphere containing 5% CO_2.

Cytotoxicity MTT assay. The colourimetric MTT assay was used to determine the toxicity of **1**-**6**. U2OS, MDA-MB-231, HeLa cells, HMLER, or HMLER-shEcad (5×10^3) were seeded in each well of a 96-well plate. After incubating the cells overnight, various concentrations of the compounds (0.2-100 µM), were added and incubated for 72 h (total volume 200 µL). Stock solutions of the compounds were prepared as 10 mM solutions in DMSO or PBS (cisplatin) and diluted using media. For compounds diluted from DMSO stock solutions, the final concentration of DMSO in each well was 0.5% and this amount was present in the untreated control as well. After 72 h, 20 µL of a 4 mg/mL solution of MTT in PBS was added to each well, and the plate was incubated for an additional 4 h. The DMEM/MTT or MEGM/MTT mixture was aspirated and 200 µL of DMSO was added to dissolve the resulting purple formazan crystals. The absorbance of the solutions in each well was read at 550 nm. Absorbance values were normalized to (DMSO-containing) control wells and plotted as concentration of test compound versus % cell viability. IC_{50} values were interpolated from the resulting dose dependent curves. The reported IC_{50} values are the average of three independent experiments, each consisting of six replicates per concentration level (overall n = 18).

Tumorsphere Formation and Viability Assay. HMLER-shEcad cells (5×10^3) were plated in ultralow-attachment 96-well plates (Corning) and incubated in MEGM supplemented with B27 (Invitrogen), 20 ng/mL EGF, and 4 µg/mL heparin (Sigma) for 5 days. Studies were conducted in the absence and presence of **2**, **6**, and cisplatin. Mammospheres treated with **2**, **6**, and cisplatin (at their respective IC_{20} values, 5 days) were counted and imaged using an inverted microscope.

Cellular Uptake. To measure the cellular uptake of **1**-**6** *ca.* 1 million HMLER-shEcad cells were treated with **1**-**6** (10 µM) at 37 ^{o}C for 3-72 h. After incubation, the media was removed, the cells were washed with PBS (2 mL × 3), harvested, and centrifuged. The cellular pellets were dissolved in 65% HNO_3 (250 µL) overnight. The samples were diluted 5-fold with water and analysed using inductively coupled plasma mass spectrometry (ICP-MS, PerkinElmer NexION 350D). Nickel levels are expressed as Ni (ppb) per million cells. Results are presented as the mean of five determinations for each data point.

RNAi Signatures. The nickel(II) complex, **2** was dosed to achieve an LD80-90 in *Eμ-Myc*$^{p19arf-/-}$ cells by propidium iodide exclusion as determined by flow cytometry after 48 h incubation. GFP enrichment/depletion was then determined by flow cytometry at 72 h. Linkage ratios (LR) and *p*-values were generated as described previously. All flow cytometry was conducted using a FACScan flow cytometer (BD Biosciences). Relatedness of **2** to other compounds in the database (including previously reported metal-based CSC-selective agents) was calculated by calculating the sum of the absolute differences of the Euclidian distances for each shRNA between the compounds. This can be represented by the following equation where C1 and C2 represent vectors of Compound 1 and Compound 2's shRNA $\log_2$(RI) values: $\sum |C1 - C2|$.

GFP Competition Assays. *Eμ-Myc*$^{p19arf-/-}$ lymphoma cells were infected with GFP-tagged shRNAs such that 15-25% of the population were GFP positive. An eighth of a million cells in 250 µL B-cell media (BCM) were then seeded into 24-well plates. For wells that would remain untreated as a control, only 1/16th of a million cells were seeded. Next, 250 µL of media containing the active agent was added to the cells. After 24 h, 300 µL of cells from untreated wells are removed and replaced by 300 µL fresh BCM. All wells then received 500 µL BCM before being placed by in the incubator for another 24 h. At 48 h, cells transduced with the control vector, MLS, were checked for viability via flow cytometry on a FACScan flow cytometer (BD Biosciences) using propidium iodide as a live/dead marker.

Immunoblotting Analysis. HMLER-shEcad cells (5×10^5 cells) were incubated with **2** (10, 15, and 20 µM for 72 h) at 37 ^{o}C. Cells were washed with PBS, scraped into SDS-PAGE loading buffer (64 mM Tris-HCl (pH 6.8)/ 9.6% glycerol/ 2% SDS/ 5% β-mercaptoethanol/ 0.01% Bromophenol Blue), and incubated at 95 ^{o}C for 10 min. Whole cell lysates were resolved by 4-20 % sodium dodecylsulphate polyacylamide gel electrophoresis (SDS-PAGE; 200 V for 25 min) followed by electro transfer to polyvinylidene difluoride membrane, PVDF (350 mA for 1 h). Membranes were blocked in 5% (w/v) non-fat milk in PBST (PBS/0.1% Tween 20) and incubated with the appropriate primary antibodies (Cell Signalling Technology). After incubation with horseradish peroxidase-conjugated secondary antibodies (Cell Signalling Technology), immune complexes were detected with the ECL detection reagent (BioRad) and analysed using a chemiluminescence imager (Amersham Imager 600).

Propidium Iodide (PI) Uptake. Untreated and treated HMLER-shEcad cells (1×10^6 cells/well) grown in six-well plates were washed with PBS (1 mL × 3), harvested, incubated with PI (5 µM for 30 min), and analysed by using a FACSCanto II flow cytometer (BD Biosciences) (10,000 events per sample were acquired). The FL2 channel was used to assess intracellular PI uptake. Cell populations were analysed using the FlowJo software (Tree Star).

JC-1 Assay. The JC-1 Mitochondrial Membrane Potential Assay Kit (Cayman) was used. The manufacturer's protocol was followed to carry out this experiment. Untreated and treated HMLER-shEcad cells (1×10^6 cells) grown in six-well plates were treated with the JC-1 staining solution for 30 min (100 µL/mL of cell media). Following staining, the cells were

harvested, and analysed using a FACSCanto II flow cytometer (BD Biosciences) (10,000 events per sample were acquired). The FL1 and FL2 channels were used to assess mitochondrial depolarisation. Cell populations were analysed using the FlowJo software (Tree Star).

Intracellular ROS Assay. HMLER-shEcad cells (5×10^3) were seeded in each well of a 96-well plate. After incubating the cells overnight, they were treated with **2** or H_2O_2 (40 and 150 μM for 6, 12, and 24 h), in the presence or absence of *N*-acetylcysteine (2.5 mM), and incubated with 6-carboxy-2′,7′-dichlorodihydrofluorescein diacetate (20 μM) for 30 min. The intracellular ROS level was determined by measuring the fluorescence of the solutions in each well at 529 nm (λ_{ex} = 504 nm).

Acknowledgements ((optional))

K.S. is supported by an Early Career Fellowship (ECF-2014-178) from the Leverhulme Trust. A.E. received financial support from a King's College London Faculty Graduate School International Studentship. C.L. thanks the Natural Science Foundation of China (Grant No.21401078) for financial support. We are grateful to Prof. Robert Weinberg for providing the HMLER and HMLER-shEcad cell lines used in this study.

Keywords: bioinorganic chemistry • nickel • necroptosis • cancer • antitumor agents

[1] a) U. Fischer, K. Schulze-Osthoff, *Cell Death Differ.* **2005**, *12 Suppl 1*, 942-961; b) J. A. Hickman, *Cancer Metastasis Rev.* **1992**, *11*, 121-139; c) D. Wang, S. J. Lippard, *Nat. Rev. Drug Discov.* **2005**, *4*, 307-320.

[2] a) M. J. Chow, M. Alfiean, G. Pastorin, C. Gaiddon, W. H. Ang, *Chem. Sci.* **2017**; b) M. J. Chow, C. Licona, G. Pastorin, G. Mellitzer, W. H. Ang, C. Gaiddon, *Chem. Sci.* **2016**, *7*, 4117-4124; c) M. Librizzi, A. Longo, R. Chiarelli, J. Amin, J. Spencer, C. Luparello, *Chem. Res. Toxicol.* **2012**, *25*, 2608-2616; d) K. Suntharalingam, S. G. Awuah, P. M. Bruno, T. C. Johnstone, F. Wang, W. Lin, Y. R. Zheng, J. E. Page, M. T. Hemann, S. J. Lippard, *J. Am. Chem. Soc.* **2015**, *137*, 2967-2974; e) S. Tardito, I. Bassanetti, C. Bignardi, L. Elviri, M. Tegoni, C. Mucchino, O. Bussolati, R. Franchi-Gazzola, L. Marchio, *J. Am. Chem. Soc.* **2011**, *133*, 6235-6242; f) S. Tian, F. M. Siu, S. C. Kui, C. N. Lok, C. M. Che, *Chem. Commun.* **2011**, *47*, 9318-9320; g) J. Yuan, Z. Lei, X. Wang, F. Zhu, D. Chen, *Metallomics* **2015**, *7*, 896-907.

[3] a) S. J. Dixon, K. M. Lemberg, M. R. Lamprecht, R. Skouta, E. M. Zaitsev, C. E. Gleason, D. N. Patel, A. J. Bauer, A. M. Cantley, W. S. Yang, B. Morrison, B. R. Stockwell, *Cell* **2012**, *149*, 1060-1072; b) S. W. G. Tait, G. Ichim, D. R. Green, *J. Cell Sci.* **2014**, *127*, 2135-2144.

[4] T. Vanden Berghe, A. Linkermann, S. Jouan-Lanhouet, H. Walczak, P. Vandenabeele, *Nat. Rev. Mol. Cell Biol.* **2014**, *15*, 135-147.

[5] P. Vandenabeele, L. Galluzzi, T. Vanden Berghe, G. Kroemer, *Nat. Rev. Mol. Cell Biol.* **2010**, *11*, 700-714.

[6] a) Z. Cai, S. Jitkaew, J. Zhao, H. C. Chiang, S. Choksi, J. Liu, Y. Ward, L. G. Wu, Z. G. Liu, *Nat. Cell Biol.* **2014**, *16*, 55-65; b) S. Jouan-Lanhouet, F. Riquet, L. Duprez, T. Vanden Berghe, N. Takahashi, P. Vandenabeele, *Semin. Cell Dev. Biol.* **2014**, *35*, 2-13; c) J. Li, T. McQuade, A. B. Siemer, J. Napetschnig, K. Moriwaki, Y. S. Hsiao, E. Damko, D. Moquin, T. Walz, A. McDermott, F. K. Chan, H. Wu, *Cell* **2012**, *150*, 339-350.

[7] K. M. Irrinki, K. Mallilankaraman, R. J. Thapa, H. C. Chandramoorthy, F. J. Smith, N. R. Jog, R. K. Gandhirajan, S. G. Kelsen, S. R. Houser, M. J. May, S. Balachandran, M. Madesh, *Mol. Cell Biol.* **2011**, *31*, 3745-3758.

[8] Z. Su, Z. Yang, L. Xie, J. P. DeWitt, Y. Chen, *Cell Death Differ.* **2016**, *23*, 748-756.

[9] M. Dean, T. Fojo, S. Bates, *Nat. Rev. Cancer* **2005**, *5*, 275-284.

[10] a) L. V. Nguyen, R. Vanner, P. Dirks, C. J. Eaves, *Nat. Rev. Cancer* **2012**, *12*, 133-143; b) D. R. Pattabiraman, R. A. Weinberg, *Nat. Rev. Drug Discov.* **2014**, *13*, 497-512; c) Y. Shiozawa, B. Nie, K. J. Pienta, T. M. Morgan, R. S. Taichman, *Pharmacol. Ther.* **2013**, *138*, 285-293.

[11] J. Kaiser, *Science* **2015**, *347*, 226-229.

[12] J. Marx, *Science* **2007**, *317*, 1029-1031.

[13] a) M. Janikova, J. Skarda, *Neoplasma* **2012**, *59*, 6-17; b) H. Korkaya, A. Paulson, E. Charafe-Jauffret, C. Ginestier, M. Brown, J. Dutcher, S. G. Clouthier, M. S. Wicha, *PLoS Biol.* **2009**, *7*, e1000121; c) N. Takebe, P. J. Harris, R. Q. Warren, S. P. Ivy, *Nat. Rev. Clin. Oncol.* **2011**, *8*, 97-106.

[14] a) G. Farnie, F. Sotgia, M. P. Lisanti, *Oncotarget* **2015**, *6*, 30472-30486; b) Y. X. Feng, E. S. Sokol, C. A. Del Vecchio, S. Sanduja, J. H. Claessen, T. A. Proia, D. X. Jin, F. Reinhardt, H. L. Ploegh, Q. Wang, P. B. Gupta, *Cancer Discov.* **2014**, *4*, 702-715; c) R. Lamb, H. Harrison, J. Hulit, D. L. Smith, M. P. Lisanti, F. Sotgia, *Oncotarget* **2014**, *5*, 11029-11037.

[15] a) M. Al-Hajj, M. S. Wicha, A. Benito-Hernandez, S. J. Morrison, M. F. Clarke, *Proc. Natl. Acad. Sci. U.S.A.* **2003**, *100*, 3983-3988; b) A. Eramo, F. Lotti, G. Sette, E. Pilozzi, M. Biffoni, A. Di Virgilio, C. Conticello, L. Ruco, C. Peschle, R. De Maria, *Cell Death Differ.* **2008**, *15*, 504-514; c) C. Li, D. G. Heidt, P. Dalerba, C. F. Burant, L. Zhang, V. Adsay, M. Wicha, M. F. Clarke, D. M. Simeone, *Cancer Res.* **2007**, *67*, 1030-1037; d) M. E. Prince, R. Sivanandan, A. Kaczorowski, G. T. Wolf, M. J. Kaplan, P. Dalerba, I. L. Weissman, M. F. Clarke, L. E. Ailles, *Proc. Natl. Acad. Sci. U.S.A.* **2007**, *104*, 973-978; e) S. K. Singh, C. Hawkins, I. D. Clarke, J. A. Squire, J. Bayani, T. Hide, R. M. Henkelman, M. D. Cusimano, P. B. Dirks, *Nature* **2004**, *432*, 396-401.

[16] a) A. Albini, A. Bruno, C. Gallo, G. Pajardi, D. M. Noonan, K. Dallaglio, *Connect. Tissue Res.* **2015**, *56*, 414-425; b) K. Kise, Y. Kinugasa-Katayama, N. Takakura, *Adv. Drug Deliv. Rev.* **2015**.

[17] a) K. Suntharalingam, W. Lin, T. C. Johnstone, P. M. Bruno, Y. R. Zheng, M. T. Hemann, S. J. Lippard, *J. Am. Chem. Soc.* **2014**, *136*, 14413-14416; b) F. Tomao, A. Papa, L. Rossi, M. Strudel, P. Vici, G. Lo Russo, S. Tomao, *J. Exp. Clin. Cancer Res.* **2013**, *32*, 48; c) M. P. Barr, S. G. Gray, A. C. Hoffmann, R. A. Hilger, J. Thomale, J. D. O'Flaherty, D. A. Fennell, D. Richard, J. J. O'Leary, K. J. O'Byrne, *PloS One* **2013**, *8*, e54193.

[18] a) J. N. Boodram, I. J. McGregor, P. M. Bruno, P. B. Cressey, M. T. Hemann, K. Suntharalingam, *Angew. Chem. Int. Ed.* **2016**, *55*, 2845-2850; b) P. Cressey, A. Eskandari, P. Bruno, C. Lu, M. Hemann, K. Suntharalingam, *ChemBioChem* **2016**; c) A. Eskandari, J. N. Boodram, P. B. Cressey, C. Lu, P. M. Bruno, M. T. Hemann, K. Suntharalingam, *Dalton Trans.* **2016**, *45*, 17867-17873; d) M. Gonzalez-Bartulos, C. Aceves-Luquero, J. Qualai, O. Cusso, M. A. Martinez, S. Fernandez de Mattos, J. A. Menendez, P. Villalonga, M. Costas, X. Ribas, A. Massaguer, *PloS One* **2015**, *10*, e0137800; e) C. T. Lum, A. S. Wong, M. C. Lin, C. M. Che, R. W. Sun, *Chem. Commun.* **2013**, *49*, 4364-4366.

[19] A. S. Abu-Surrah, M. Kettunen, *Curr. Med. Chem.* **2006**, *13*, 1337-1357.

[20] a) Z. Afrasiabi, E. Sinn, W. Lin, Y. Ma, C. Campana, S. Padhye, *J. Inorg. Biochem.* **2005**, *99*, 1526-1531; b) J. Chen, Y. W. Huang, G. Liu, Z. Afrasiabi, E. Sinn, S. Padhye, Y. Ma, *Toxicol. Appl. Pharmacol.* **2004**, *197*, 40-48.

[21] F. Liang, P. Wang, X. Zhou, T. Li, Z. Li, H. Lin, D. Gao, C. Zheng, C. Wu, *Bioorg. Med. Chem. Lett.* **2004**, *14*, 1901-1904.

[22] a) A. Shrivastav, N. K. Singh, S. M. Singh, *Bioorg. Med. Chem.* **2002**, *10*, 887-895; b) A. Shrivastav, N. K. Singh, S. M. Singh, *Biometals* **2003**, *16*, 311-320.

[23] C. Zhao, X. Chen, D. Zang, X. Lan, S. Liao, C. Yang, P. Zhang, J. Wu, X. Li, N. Liu, Y. Liao, H. Huang, X. Shi, L. Jiang, X. Liu, Z. He, Q. P. Dou, X. Wang, J. Liu, *Oncogene* **2016**, *35*, 5916-5927.

[24] F. P. Emmenegger, *Inorg. Chem.* **1989**, *28*, 2210-2214.

[25] P. B. Gupta, T. T. Onder, G. Jiang, K. Tao, C. Kuperwasser, R. A. Weinberg, E. S. Lander, *Cell* **2009**, *138*, 645-659.

[26] G. Dontu, W. M. Abdallah, J. M. Foley, K. W. Jackson, M. F. Clarke, M. J. Kawamura, M. S. Wicha, *Genes Dev* **2003**, *17*.

[27] a) H. Jiang, J. R. Pritchard, R. T. Williams, D. A. Lauffenburger, M. T. Hemann, *Nat. Chem. Biol.* **2011**, *7*, 92-100; b) J. R. Pritchard, P. M. Bruno, L. A. Gilbert, K. L. Capron, D. A. Lauffenburger, M. T. Hemann, *Proc. Natl. Acad. Sci. U.S.A.* **2013**, *110*, E170-179; c) J. R. Pritchard, P. M. Bruno, M. T. Hemann, D. A. Lauffenburger, *Mol. Biosyst.* **2013**, *9*, 1604-1619.

[28] W. Han, L. Li, S. Qiu, Q. Lu, Q. Pan, Y. Gu, J. Luo, X. Hu, *Mol. Cancer Ther.* **2007**, *6*, 1641-1649.

[29] K. Dodo, M. Katoh, T. Shimizu, M. Takahashi, M. Sodeoka, *Bioorg. Med. Chem. Lett.* **2005**, *15*, 3114-3118.

[30] a) A. Degterev, J. Hitomi, M. Germscheid, I. L. Ch'en, O. Korkina, X. Teng, D. Abbott, G. D. Cuny, C. Yuan, G. Wagner, S. M. Hedrick, S. A. Gerber, A. Lugovskoy, J. Yuan, *Nat. Chem. Biol.* **2008**, *4*, 313-321; b) A. Degterev, Z. Huang, M. Boyce, Y. Li, P. Jagtap, N. Mizushima, G. D. Cuny, T. J. Mitchison, M. A. Moskowitz, J. Yuan, *Nat. Chem. Biol.* **2005**, *1*, 112-119; c) J. X. Li, J. M. Feng, Y. Wang, X. H. Li, X. X. Chen, Y. Su, Y. Y. Shen, Y. Chen, B. Xiong, C. H. Yang, J. Ding, Z. H. Miao, *Cell Death Dis.* **2014**, *5*, e1278.

[31] E. A. Slee, H. Zhu, S. C. Chow, M. MacFarlane, D. W. Nicholson, G. M. Cohen, *Biochem. J.* **1996**, *315 (Pt 1)*, 21-24.

[32] a) K. Moriwaki, J. Bertin, P. J. Gough, G. M. Orlowski, F. K. Chan, *Cell Death Dis.* **2015**, *6*, e1636; b) H. Sawai, *Int. J. Mol. Sci.* **2016**, *17*; c) F. Basit, S. Cristofanon, S. Fulda, *Cell Death Differ.* **2013**, *20*, 1161-1173.

[33] H. Wang, L. Sun, L. Su, J. Rizo, L. Liu, L. F. Wang, F. S. Wang, X. Wang, *Mol. Cell* **2014**, *54*, 133-146.

[34] L. Sun, H. Wang, Z. Wang, S. He, S. Chen, D. Liao, L. Wang, J. Yan, W. Liu, X. Lei, X. Wang, *Cell* **2012**, *148*, 213-227.

[35] a) S. He, L. Wang, L. Miao, T. Wang, F. Du, L. Zhao, X. Wang, *Cell* **2009**, *137*, 1100-1111; b) V. Temkin, Q. Huang, H. Liu, H. Osada, R. M. Pope, *Mol. Cell Biol.* **2006**, *26*, 2215-2225.

[36] S. T. Smiley, M. Reers, C. Mottola-Hartshorn, M. Lin, A. Chen, T. W. Smith, G. D. Steele, Jr., L. B. Chen, *Proc. Natl. Acad. Sci. U.S.A.* **1991**, *88*, 3671-3675.

[37] a) Y. S. Cho, S. Challa, D. Moquin, R. Genga, T. D. Ray, M. Guildford, F. K. Chan, *Cell* **2009**, *137*, 1112-1123; b) C. W. Davis, B. J. Hawkins, S. Ramasamy, K. M. Irrinki, B. A. Cameron, K. Islam, V. P. Daswani, P. J. Doonan, Y. Manevich, M. Madesh, *Free Radic. Biol. Med.* **2010**, *48*, 306-317; c) D. W. Zhang, J. Shao, J. Lin, N. Zhang, B. J. Lu, S. C. Lin, M. Q. Dong, J. Han, *Science* **2009**, *325*, 332-336.

[38] a) J. Sosna, S. Voigt, S. Mathieu, A. Lange, L. Thon, P. Davarnia, T. Herdegen, A. Linkermann, A. Rittger, F. K. Chan, D. Kabelitz, S. Schutze, D. Adam, *Cell Mol. Life. Sci.* **2014**, *71*, 331-348; b) X. Xu, C. C. Chua, M. Zhang, D. Geng, C. F. Liu, R. C. Hamdy, B. H. Chua, *Brain Res.* **2010**, *1343*, 206-212.

[39] R. Chavez-Valdez, L. J. Martin, F. J. Northington, *Neurol. Res. Int.* **2012**, *2012*, 257563.

[40] C. K. Donawho, Y. Luo, Y. Luo, T. D. Penning, J. L. Bauch, J. J. Bouska, V. D. Bontcheva-Diaz, B. F. Cox, T. L. DeWeese, L. E. Dillehay, D. C. Ferguson, N. S. Ghoreishi-Haack, D. R. Grimm, R. Guan, E. K. Han, R. R. Holley-Shanks, B. Hristov, K. B. Idler, K. Jarvis, E. F. Johnson, L. R. Kleinberg, V. Klinghofer, L. M. Lasko, X. Liu, K. C. Marsh, T. P. McGonigal, J. A. Meulbroek, A. M. Olson, J. P. Palma, L. E. Rodriguez, Y. Shi, J. A. Stavropoulos, A. C. Tsurutani, G. D. Zhu, S. H. Rosenberg, V. L. Giranda, D. J. Frost, *Clin. Cancer Res.* **2007**, *13*, 2728-2737.

[41] M. Banasik, H. Komura, M. Shimoyama, K. Ueda, *J. Biol. Chem.* **1992**, *267*, 1569-1575.

[42] S. Park, S. P. Yoon, J. Kim, *Anat. Cell Biol.* **2015**, *48*, 66-74.

[43] Cotton, F. A.; McCleverty, J. A., *Inorg. Chem.* **1964**, 3 (10), 1398-1402.

Entry for the Table of Contents (Please choose one layout)

Layout 1:

FULL PAPER

Killing cancer stem cells another way: Multi-drug resistant pathways, including apoptosis dysfunction, are operative in cancer stem cells (CSCs), and thus apoptosis-inducing chemotherapies are largely ineffective against this class of cancer cells. Therefore, the discoveries of chemical agents that can induce CSC death through non-apoptotic pathways are highly valuable in the fight against cancer. Here we report the first nickel complex to induce CSC death by necroptosis, an ordered form of necrosis.

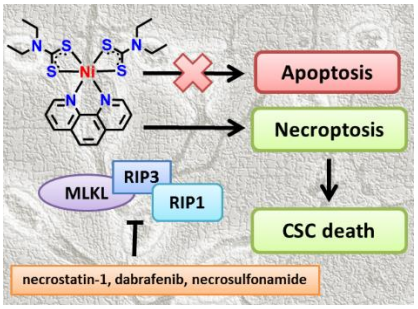

*Author(s), Corresponding Author(s)**

Page No. – Page No.

Title